
Since January 2020 Elsevier has created a COVID-19 resource centre with free information in English and Mandarin on the novel coronavirus COVID-19. The COVID-19 resource centre is hosted on Elsevier Connect, the company's public news and information website.

Toxicology and Applied Pharmacology 434 (2022) 115796

Contents lists available at ScienceDirect

Toxicology and Applied Pharmacology

journal homepage: www.elsevier.com/locate/taap

# Non-clinical safety assessment and *in vivo* biodistribution of CoviFab, an RBD-specific F(ab′)2 fragment derived from equine polyclonal antibodies

Facundo Salinas [a,1], Belkis E. Marelli [a,b,1], Santiago Sanguineti [c], Fernando Goldbaum [c,d,e], Luciana Muñoz [c], Lucas Etchevers [a], Paula Silvestrini [a], Ulises S. Notaro [a], Natalia R. Salvetti [a,b], Vanesa Zylberman [c,f,2], Hugo H. Ortega [a,b,*,2]

[a] Centro de Medicina Comparada, Instituto de Ciencias Veterinarias del Litoral (ICiVet-Litoral), Universidad Nacional del Litoral (UNL) / Consejo Nacional de Investigaciones Científicas y Técnicas (CONICET), Esperanza, Santa Fe, Argentina
[b] Facultad de Ciencias Veterinarias del Litoral, Universidad Nacional del Litoral (UNL), Esperanza, Santa Fe, Argentina
[c] INMUNOVA S.A., Av. Patricias Argentinas 435, Ciudad de Buenos Aires C1405BWE, Argentina
[d] CRIP-Centro de Rediseño e Ingeniería de Proteínas UNSAM, Campus Miguelete, San Martín, Provincia de Buenos Aires, Argentina
[e] Laboratorio de Inmunología y Microbiología Molecular, Fundación Instituto Leloir, IIBBA-CONICET, Buenos Aires, Argentina
[f] Consejo Nacional de Investigaciones Científicas y Técnicas, (CONICET), Argentina

ARTICLE INFO

Editor: Lawrence Lash

*Keywords:*
CoviFab
Preclinical studies
Biodistribution
Good laboratory practices
COVID-19

ABSTRACT

The severe acute respiratory syndrome coronavirus 2 (SARS-CoV-2) has required the urgent development of new therapies, among which passive immunotherapy is contemplated. CoviFab (INM005) is a RBD-specific F(ab′)2 fragment derived from equine polyclonal antibodies. We investigate their preclinical security and biodistribution by *in vivo* and *ex vivo* NIR imaging after intravenous administration of a dose of 4 mg/kg at time 0 and 48 h. Images were taken at 1, 12, 24, 36, 48, 49, 60, 72, 84, 96, 108, 120, 132 and 144 h after the first intravenous injection. At 96 and 144 h, mice were sacrificed for haematology, serum chemistry, clinical pathology, histopathology and *ex vivo* imaging. The biodistribution profile was similar in all organs studied, with the highest fluorescence at 1 h after each injection, gradually decreasing after that each one and until the end of the study (144 h). The toxicology study revealed no significant changes in the haematology and serum chemistry parameters. Further, there were no changes in the gross and histological examination of organs. Nonclinical data of the current study confirm that CoviFab is safe, without observable adverse effects in mice. Furthermore, we confirm that bioimaging studies are a useful approach in preclinical trials to determine biodistribution.

## 1. Introduction

The severe acute respiratory syndrome coronavirus 2 (SARS-CoV-2), an emerging human coronavirus, was discovered in Wuhan, China, in 2019. It causes COVID-19 (coronavirus-induced disease of 2019), which developed into a pandemic in early 2020 and has affected and continues to affect millions of people, despite the tremendous social preventive measures taken worldwide (Sallard et al., 2020a).

The search for the most effective therapy against COVID-19 has driven the research of several different forms of treatment, including antivirals (Choy et al., 2020; Pizzorno et al., 2020; Shannon et al., 2020), a combination of interferons (Sallard et al., 2020b), corticosteroids (Li et al., 2020; Zha et al., 2020), protease inhibitors (Jiménez-Alberto et al., 2020; Khan et al., 2020), convalescent plasma (Chai et al., 2020; Farrugia et al., 2020), ivermectin (Gupta et al., 2020; Heidary and Gharebaghi, 2020), monoclonal, and polyclonal antibodies, as well as vaccines (da Costa et al., 2021).

Some of these therapies have provided benefits in the treatment of patients with COVID-19 infection. Among them, passive immunotherapy is one of the alternatives explored for treating coronavirus infections. It has been used in medical practice for many years (Berry and Gaudet, 2011) and stands out as a possibility in the current pandemic scenario (Bonam et al., 2020). It is a treatment that aims at inducing immunity in a short time and is extremely relevant as a therapy of choice

* Corresponding author at: Instituto de Ciencias Veterinarias del Litoral (ICIVET Litoral, UNL-CONICET), R. P. Kreder 2805, 3080 Esperanza, Santa Fe, Argentina.
*E-mail address:* hhortega@fcv.unl.edu.ar (H.H. Ortega).
[1] F Salinas and BE Marelli should be considered a joint first author.
[2] V Zylberman and Ortega HH should be considered a joint senior author.

https://doi.org/10.1016/j.taap.2021.115796
Received 30 April 2021; Received in revised form 16 October 2021; Accepted 10 November 2021
Available online 14 November 2021

in a pandemic (da Costa et al., 2021; Lotfi et al., 2020). In this sense, passive immunisation treatments aim to increase the patient's immune response, preventing the disease from progressing to more severe conditions (Gasparyan et al., 2020). Equine polyclonal antibodies have been used for decades in the management of clinical emergencies, such as snakebite and scorpion sting envenomation, severe poisoning (tetanus toxin, digoxin, and, more recently, botulinum toxin), and severe infectious diseases like avian influenza (Bal et al., 2015; Herbreteau et al., 2014; Lang et al., 1998; Quiambao et al., 2008). Considering the magnitude of social and economic problems arising from the COVID-19 pandemic, Inmunova S.A. developed a therapy named CoviFab (INM005) based on equine polyclonal antibodies (EpAbs). CoviFab recognises a vast array of epitopes (limiting the risk of viral escape mutations) and tends to develop greater avidity than monoclonal antibodies (mAbs) for their cognate antigens (Zylberman et al., 2020). In this sense, CoviFab as well as convalescent plasma (CP), contains anti-RBD neutralizing activity. However, some important differences between these two passive immunotherapies should be highlighted. The Fc region of specific anti-spike IgG was associated with acute lung injury in SARS-CoV-2 infection (Liu et al., 2019) and CP may be associated with the antibody-dependent enhancement (ADE) effect. In this sense, F(ab′)2 fragments retain the bivalent binding ability of IgG antibodies while avoiding the potential ADE consequence, due to the lack of the Fc region (Wu et al., 2020; Lee et al., 2020). Therefore, in patients with a severe disease, these differences might explain why CoviFab, and not CP therapy, might be associated with better outcomes in well controlled clinical trials (Simonovich et al., 2021; Lopardo et al., 2021).

The CoviFab development employs a strategy similar to the therapy based on Neutralising Equine Anti Shiga Toxin (NEAST) F(ab′)2 fragment antibodies for the prevention of the haemolytic-uremic syndrome (Hiriart et al., 2019). The NEAST therapy has successfully passed preclinical and phase 1 analysis, showing an adequate safety and pharmacokinetics profile. Its positive evaluation enabled the initiation of a 2/3-phase clinical trial in the paediatric population, which is currently ongoing (http://www.clinicaltrials.gov, NCT04132375) (Lopardo et al., 2021) and, therefore, it is in the process of registration in several regulatory agencies such as the National Administration of Drugs, Food, and Medical Technology (ANMAT) and European Medicines Agency (EMA).

Taking into account this safety and pharmacokinetic background, and given the similarity of the F(ab′)2 molecules, the Argentine regulatory authorities ANMAT authorised a 2/3-phase clinical trial (http://www.clinicaltrials.gov, NCT04494984) for CoviFab and its registration and emergency approval (Lopardo et al., 2021).

The objective of this study was to investigate the preclinical safety and biodistribution of CoviFab after intravenous administration. To test this, we evaluated haematology, serum chemistry, clinical pathology, histopathology, biodistribution, and persistence in a comprehensive panel of organs and tissues. These studies provided additional preclinical safety and biodistribution data for the evaluation of CoviFab administration to COVID patients.

## 2. Material and methods

### 2.1. Equine polyclonal antibodies (EpAbs) CoviFab (INM005) production

CoviFab was produced and purified according to Good Manufacturing Practices (GMP) (Hiriart et al., 2019; Zhang et al., 2020; Zylberman et al., 2020). Briefly, the recombinant receptor-binding domain protein (RBD) of SARS-CoV-2 was produced using the mammalian expression plasmid pCAGGS, which was kindly provided by Prof. Florian Krammer (Amanat et al., 2020). This plasmid contains the coding region for RBD (Spike residues 319–541) along with a signal peptide (residues 1–14) and a C-terminal hexahistidine tag. The plasmid was transfected into human embryonic kidney (HEK) 293T cells (ATCC CRL-3216, USA) as an expression system. RBD was purified by affinity chromatography and then was checked by SDS-PAGE in both reducing and non-reducing conditions and by analytical size exclusion chromatography.

Horses were immunised as described previously, and the first batch was released under the same GMP standard used for other equine hyperimmune sera produced at the *Instituto Biológico Argentino* (Argentina) (Zylberman et al., 2020).

The antibody response was determined by an indirect ELISA using purified RBD as the antigen, and the *in vitro* neutralisation capacity was checked using a seroneutralisation assay against SARS-CoV-2. F(ab′)2 fragments were processed and purified as described by Zylberman et al. (2020).

### 2.2. Conjugation of CoviFab with NIR dyes and western blot

CoviFab (Lot 6454, concentration 43.8 mg/ml) was diluted at 1 mg/ml in Buffer Saline Phosphate (PBS), and 1 mg was conjugated with IRDye 800CW Protein Labeling Kit – High MW (LI-COR Biosciences Inc., Lincoln, NE) following manufacturer's instructions. Excess dye was removed using a Zeba desalting column (Thermo Fisher Scientific, Waltham, MA), and the product was suspended in PBS. Protein concentration was measured using the Lowry method on a microplate reader (BioRad Laboratories Inc., Hercules, CA). Finally, the concentration was adjusted to 0.8 mg/ml with PBS.

Amounts of 5, 1, 0.5, and 0.1 μg protein were separated using 8% SDS-PAGE gel electrophoresis in native (non-denatured) conditions. The gel was observed in a Pearl Trilogy Fluorescence Imaging system (LI-COR Biosciences), and the proteins were visualised by scanning the gel with the 800-nm channel (Fig. 1A).

### 2.3. Non-clinical safety and quantitative in vivo biodistribution in mice

All the procedures were carried out according to the Guide for the Care and Use of Laboratory Animals (National Research Council, 2011) and with the approval of the Institutional Ethics and Security Committee (Protocol N° 632/20) of the School of Veterinary Science of the National University of Litoral, Santa Fe, Argentina. The Centre for Comparative Medicine is an entity compliant with GLP for conducting preclinical tests inspected by the Argentine Accreditation Organism (member of the OECD) and the certifications of local regulatory agencies like the ANMAT and the SENASA (National Argentine Service of Animal Sanitation and Food Quality).

Adult BALB/cCmedc mice (males, 6–7 weeks, 21.1 ± 1.5 g, $n = 13$) were housed in individually ventilated cage (IVC) systems (Allentown Inc., USA) and given food and water *ad libitum*. The temperature of the animal facility was 23 °C with a 12-h light/dark cycle. Animals were divided into two groups consisting of a treated group ($n = 8$) and a control group ($n = 5$).

To evaluate the safety and biodistribution of repeated administrations of CoviFab, a dose of 4 mg/kg was administered to the treated animals via intravenous tail-vein injection (5 ml/kg) at time 0 and at 48 h. This dose and application scheme coincide with the ones used in the clinical trial, based on the therapeutic dose of similar products (Lopardo et al., 2021). Control animals received sterile sodium chloride solution (0.9% w / v in water).

The animals were observed twice daily for clinical evolution, viability/mortality and for any change in behaviour or reaction to treatment. The food and water consumption were monitored once during the assay period. Body weights were recorded every 48 h.

Mice imaging was carried out using a Pearl Trilogy Small Animal Fluorescence Imaging System and the Image Studio software V 5.2 for data capture and analysis. The presence of IRDye conjugated CoviFab was detected using an excitation wavelength of 785 nm and an emission filter of 820 nm.

To obtain the images, the animals were anesthetized with 5% isofluorane for induction, and 2% for maintenance of the anaesthetic plane.

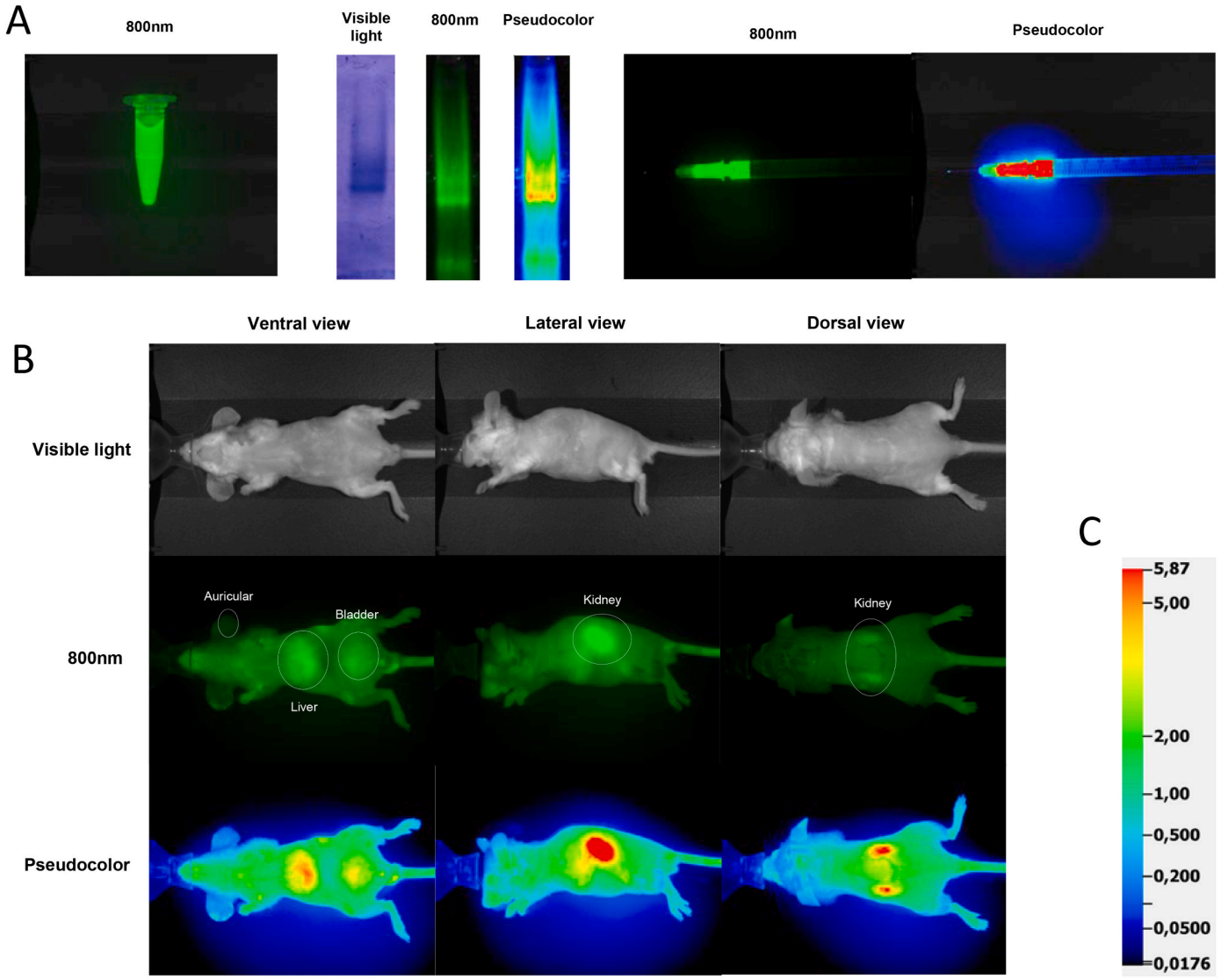


**Fig. 1.** A: Preparation and characterisation of CoviFab labelled with IRDye® 800CW: electrophoretic profile at visible light, infrared (800 nm), and pseudocolour showing the specific binding to F(ab′)2 fragment derived from equine polyclonal antibodies, and the detail of a syringe loaded with a dose. B: Observation with visible light, infrared (800 nm), and pseudocolour of the three captured views of each animal (ventral, lateral, and dorsal) and the areas analysed in each one (auricular, liver, kidney, and bladder). C: Scale used for the generation of pseudocolour images.

In treated animals, images were taken at 1, 12, 24, 36, 48, 49, 60, 72, 84, 96, 108, 120, 132, and 144 h after the first intravenous injection. The images at 48 h were taken before the second administration of CoviFab. Control animals were imaged at T0 to establish the basal level of fluorescence. This sampling frequency was selected based on pharmacokinetic data from other F(ab′)2 fragments (Hiriart et al., 2019). Images of ventral, lateral, and dorsal views were collected to obtain a direct projection of auricular, liver, bladder, and kidney areas, for subsequent fluorescence analysis as described below (Fig. 1B). Those organs were studied because they had the highest fluorescence (target organs). The auricular region was used to obtain data about the biodistribution in peripheral tissues. Faeces and urine were also collected and analysed as indicators of elimination.

The images were analysed using the Image Studio V5.2 software. Regions of interest (ROI) for auricular, liver, bladder, and kidney areas were selected from areas containing the regions of projection of these organs. The ROIs were quantified according to the maximum value of the pixels within the shape limits. The software determines arbitrary units for the quantification of the fluorescence intensity (RFU: relative fluorescence units). Because pseudo-coloured images can distinguish different intensities easier, some images with fluorescence signals were also presented in pseudocolour (Fig. 1B).

### 2.4. Necropsy and ex vivo organ imaging

After final imaging at 96 and 144 h, 4 mice of the experimental group were sacrificed at each time by anaesthetic overdose. Also, control animals ($n = 5$) were euthanised 144 h after the administration of the same volume of saline solution. Before the necropsy, blood samples for haematology, serum chemistry, and F(ab′)2 quantification were obtained through cardiac puncture.

A complete necropsy was carried out, including organ weights and gross pathology. The heart, lung (with bronchi), liver, spleen, and kidney were removed and weighed. The organ/body weight ratios (relative weight) were calculated using the terminal body weight obtained prior to the necropsy. Paired organs were weighed together.

For *ex vivo* analysis, the following organs were collected: liver, kidney, adrenal glands, stomach/intestine, testicles, spleen, lung, heart, brain, eyes, bladder, and blood. Organs were rapidly dissected and placed under the Pearl Trilogy system for analysis, and images were

acquired and analysed as described above.

### 2.5. Histopathological analysis

Samples of liver, kidney, adrenal, testis and epididymis, lung, heart, and brain were fixed in 4% buffered formaldehyde for 8–10 h at 25 °C and then washed in PBS. Then, fixed tissues were dehydrated in an ascending series of ethanol, cleared in xylene and embedded in paraffin. Sections (5 μm thick) were mounted on slides previously treated with 2% (*v*/v) 3-aminopropyltriethoxysilane in acetone (Sigma-Aldrich, St. Louis, MO, USA) and stained with haematoxylin-eosin. Microscopic images were digitised with a CCD colour video camera Nikon DS-Fi2 mounted on a conventional light microscope Nikon Eclipse Ci-L Ni (Tokyo, Japan) and examined by a veterinary pathologist.

### 2.6. Haematology and serum chemistry

Collected blood samples were stored in tubes with EDTA and analysed by an automated haematology analyser (Mindray BC-2800Vet, China). Haematologic parameters were analysed, including red blood cells (RBC), haematocrit (HCT), haemoglobin (HGB), mean cell volume of red blood cells (MCV), mean cell haemoglobin (MCH), mean corpuscular haemoglobin concentration (MCHC), platelet (PLT), white blood cells (WBC) with differential count of granulocytes (GRA), lymphocytes (LYM), and monocytes (MNO).

Blood was also taken for serum chemistry in glass tubes, then placed for approximately 30 min at room temperature, and the serum was obtained by centrifugation at 3000 rpm for 10 min. Clinical chemistry was determined with validated micro-methods for small volumes, with commercial kits (Wiener Labs, Argentina) and a microplate reader (SPECTROStar Nano, BMG Labtech, Germany). Blood urea nitrogen (BUN), creatinine (CRE), alanine aminotransferase (ALT), aspartate aminotransferase (AST), total protein (TP), albumin (ALB), globulins (GLO), and glucose (GLU) were measured.

### 2.7. ELISA for equine F(ab′)2

This method has been previously developed and validated according to FDA guidelines (Guidance for Industry: Bioanalytical Method Validation, FDA, 2018) to determine the concentration of equine F(ab′)2 in serum samples from different species including mice (Hiriart et al., 2019; Lopardo et al., 2021). The method consisted of sandwich ELISA, in which the samples were incubated in a plate coated with an anti-equine F(ab′)2 antibody (LS-C60458, LS Bio, USA), and revealed by the addition of an anti-equine immunoglobulins antibody conjugated with peroxidase (SC-2448, Santa Cruz USA). Finally, a chromogenic substrate (TMB, 3,3′,5,5′-tetramethylbenzidine, Life Technologies, USA) was added, and the absorbance was read at 450 nm using a microplate reader (SPECTROstar Nano, BMG Labtech, Germany). The signal was interpolated in a standard curve evaluated in the same assay and adjusted to a multiparameter model. In mouse samples, this method has an average intra-assay coefficient of variation (CV) of 5.67% and an inter-assay CV of 7.49%.

### 2.8. Statistical analysis

Statistical analysis was performed using SPSS Statistics, version 24 (IBM, Armonk, NY). The presented data are shown as mean +/− standard error of mean (SEM). For all data, normality was determined by the Shapiro-Wilk test, and the homogeneity of variances was tested with Levene's test.

The one-way ANOVA test was used to compare means between groups at each time point. If the group effect of the ANOVA was significant ($P < 0.05$), Dunnett's test was used for pairwise comparisons between each set of treated and control groups or against basal values.

The correlation coefficient between *ex vivo* fluorescence imaging of organs, fluorescence analysis of urine and faeces, and serum F(ab′)2 concentration at basal (controls), 96 and 144 h was calculated according to the Pearson correlations test. Statistical significance was set at $P < 0.05$.

## 3. Results

To evaluate the preclinical security and the biodistribution of CoviFab, a series of haematology, serum chemistry, clinical pathology, histopathology, and *in vivo* and *ex vivo* NIR imaging studies were performed in a comprehensive panel of organs and tissues of mice.

### 3.1. Non-clinical safety and in vivo biodistribution in mice

Treated and control groups were examined daily for general appearance, behaviour, signs of toxicity, morbidity, and mortality. No mortality was observed during the study period. All the animals of both the treated and the control groups remained active and healthy during the experiment period.

Bodyweight did not change significantly in the CoviFab treatment groups by comparison with the vehicle control group (Table 1). No significant differences were observed in the treated animals over time and, when comparing the bodyweight at 144 h with the preadministration basal weight, the percentage of difference was at −2.7% ($P = 0.16$).

The *in vivo* biodistribution of labelled CoviFab is presented in Fig. 2. Following the intravenous injections, CoviFab was distributed in all the areas studied. The highest fluorescence intensity was observed 1 h after each administration (1 and 49 h imaging), gradually decreasing thereafter. Fluorescent signals were predominantly detected *in vivo* in the regions of the kidney, liver, and bladder, and little or no signal was detected in basal observation (background fluorescence).

Fluorescent signals were detected in the renal areas at dorsal and lateral views. Twenty-four hours after the first administration and 36 h after the second administration (84 h observation), a stronger signal was detected in renal areas compared to control ($P < 0.05$; Fig. 2). After both administrations and until the 120 h, a higher fluorescent signal was detected in the liver region compared to control ($P < 0.05$; Fig. 2). Quantification results revealed significantly stronger signals ($P < 0.05$; Fig. 2) in the bladder area up to 24 h after the first administration and 12 h (60 h observation) after the second. Moreover, while analysing the auricular region as an indicator of the presence of the labelled CoviFab in the peripheral circulation, a signal higher than the basal ($P < 0.05$; Fig. 2) was found until the 108 h observation.

A stronger fluorescence signalling was observed in urine 1 h and 12 h after the first administration and 1 h after the second administration (49 h observation) compared to control ($P < 0.05$; Fig. 3). Also, 1 h after the second administration (49 h observation), significantly stronger fluorescence was observed in faeces ($P < 0.05$; Fig. 3).

### 3.2. Necropsy, organ weights and histopathological analysis

The postmortem complete macroscopic examination revealed no tissue change in CoviFab-treated animals. The relative organ weights did not evidence significant differences compared to the control group

**Table 1**
Animal weight (g) at different times of mice treated with CoviFab and controls.

| Control animals ($n = 5$) | Treated animals | | | |
|---|---|---|---|---|
| | Basal ($n = 8$) | 48 h ($n = 8$) | 96 h (n = 8) | 144 h ($n = 4$) |
| 21.7 ± 0.5 | 21.1 ± 1.5 | 20.8 ± 1.9 | 20.8 ± 1.8 | 19.7 ± 1.8 |

Data are presented as mean ± standard deviations. No statistically significant differences compared with the vehicle control group at $P < 0.05$ were observed (analysis of variance, Dunnett post hoc test).

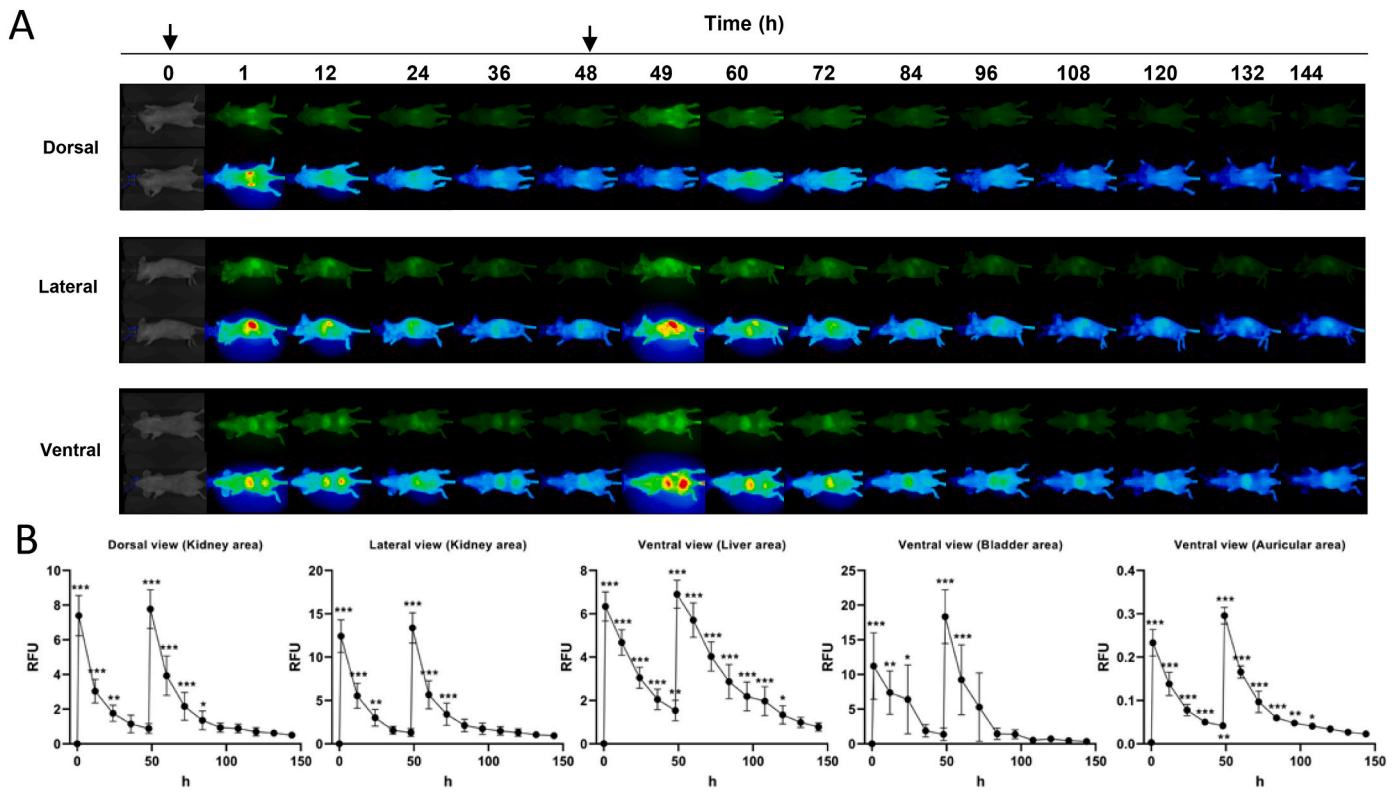


**Fig. 2.** *In vivo* biodistribution of CoviFab labelled with IRDye® 800CW in mice, after the administration of intravenous doses of 4 mg/kg at time 0 and 48 h. A: Representative images acquired at different times and observed at 800 nm (top) and pseudocolour (bottom) of ventral, lateral, and dorsal views. The arrows indicate the days when the treatments were performed. B: Biodistribution profile based on the quantitative analysis of fluorescence (RFU: relatives fluorescence units) in auricular, liver, kidney, and bladder areas (details in Fig. 1). Data are presented as mean ± standard deviations. Significant differences with vehicle control group (0) (analysis of variance, Dunnett post hoc test) are indicated (* = $p < 0.05$; ** = $p < 0.01$; *** = $p < 0.001$).

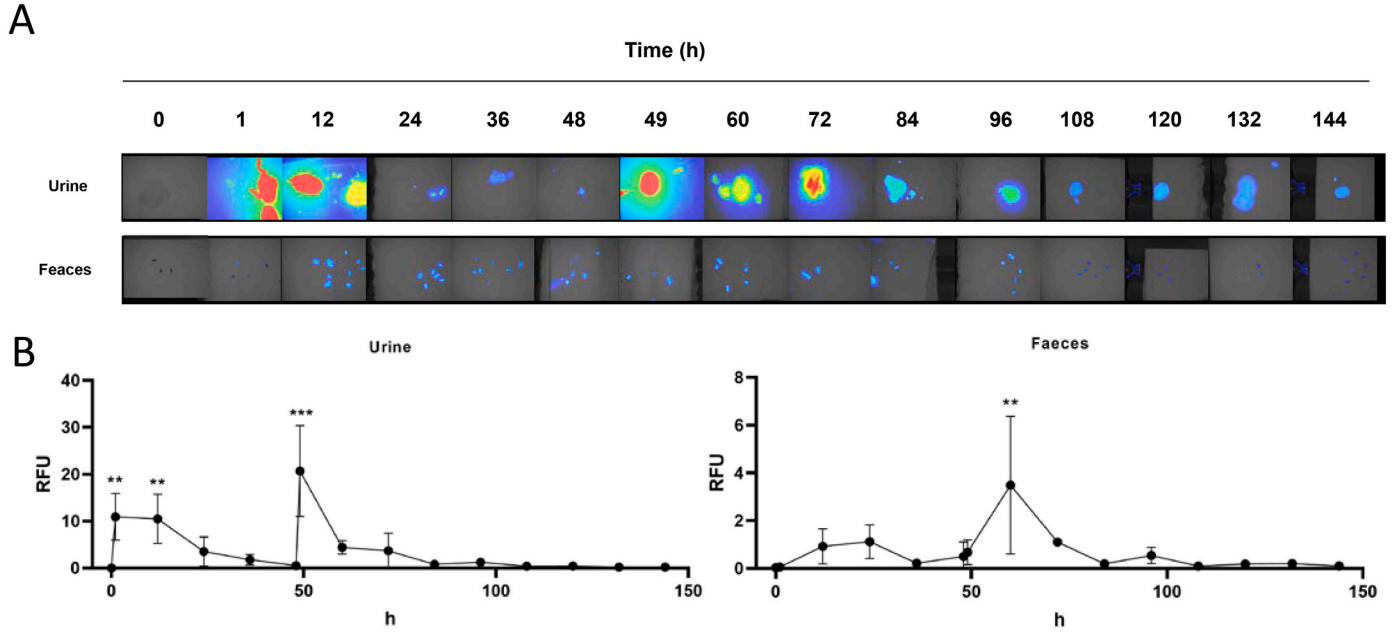


**Fig. 3.** Fluorescence analysis of urine and faeces samples as indicators of elimination of CoviFab labelled with IRDye® 800CW in mice, after the administration of intravenous doses of 4 mg/kg at time 0 and at 48 h. A: Representative pseudocolour images acquired at different times. B: Quantitative analysis of fluorescence (RFU: relatives fluorescence units). Data are presented as mean ± standard deviations. Significant differences with vehicle control group (0) (analysis of variance, Dunnett post hoc test) are indicated (** = $p < 0.01$; *** = $p < 0.001$).

**Table 2**
Relative organ weights (organ/body weight ratios (%)) of mice treated with CoviFab and controls.

| Organs | Control animals (n = 5) | Treated animals | |
|---|---|---|---|
| | | 96 h (n = 4) | 144 h (n = 4) |
| Heart | 0.566 ± 0.127% | 0.591 ± 0.072% | 0.587 ± 0.058% |
| Lung | 0.808 ± 0.169% | 0.944 ± 0.069% | 0.978 ± 0.146% |
| Liver | 4.524 ± 0.181% | 4.915 ± 0.280% | 4.820 ± 0.377% |
| Spleen | 0.324 ± 0.019% | 0.293 ± 0.028% | 0.329 ± 0.069% |
| Kidney | 1.661 ± 0.177% | 1.779 ± 0.087% | 1.740 ± 0.055% |

Data are presented as mean ± standard deviations. No statistically significant differences compared with vehicle control group at $P < 0.05$ were observed (analysis of variance, Dunnett post hoc test).

(Table 2). There were no treatment-related effects on histology and all the organs studied were normal without microscopic lesions (Fig. 4).

### 3.3. Ex vivo organ imaging

The *ex vivo* imaging analysis was designed to confirm the findings from *in vivo* CoviFab labelled imaging study. The fluorescent signals detected at 96 h in the liver, kidney, adrenal glands, stomach/intestine, testicles, spleen, lung, heart, brain, eyes, bladder, and blood showed significant differences compared to control ($P < 0.05$; Fig. 4). The higher signals were detected in the liver, followed by the kidney ($P < 0.001$). At 144 h, statistically significant signals were detected in the liver, kidney, adrenal glands, stomach/intestine, testicles, spleen, and heart ($P < 0.05$; Fig. 5).

### 3.4. Haematology, serum chemistry and serum F(ab')2

As shown in Table 3, CoviFab treated groups showed no significant ($P > 0.05$) changes in haematological parameters. Haematological biomarker counts such as RBC, HCT, HGB, MCV, MCH, MCHC, PLT, WBC, GRA, LYM, and MNO in treated groups were within the normal range when compared to the control group. Moreover, the serum chemistry profile (BUN, CRE, ALT, AST, TP, ALB, GLO and GLU) also was within the normal range when compared to the control group ($P > 0.05$; Table 4).

The serum concentration of CoviFab after the administration of two doses of 4 mg/kg was 17.07 ± 3.40 mg/L and 6.1 ± 1.25 mg/L at 96 and 144 h, respectively (Table 4).

### 3.5. Correlation analysis of fluorescence and serum CoviFab concentration

To assess the relation between the *ex vivo* fluorescence of organs, the fluorescence of urine and faeces, and serum F(ab')2 at basal, 96 and 144 h, a correlation analysis was performed. A complete Pearson's correlation matrix of the results is presented in Table 5.

A positive linear correlation (Pearson's correlation coefficient $r > 0.7$) among all the parameters analysed was found. The intensity of fluorescence signalling in liver, lung, heart, eyes, and blood showed a positive correlation with serum F(ab')2 concentration ($r > 0.95$; $P < 0.05$). Moreover, positive correlations were observed between fluorescence in different organs, urine, and faeces ($r > 0.95$; $P < 0.05$) (Table 5).

## 4. Discussion and conclusions

Although progress with the application of vaccines and other therapeutic measures is being made, the COVID-19 widespread pandemic continues to spread all across the globe, with high mortality rates and especially in high-risk patients, which currently constitutes a major public health concern (Artese et al., 2020; Bayat et al., 2021; Twomey et al., 2020). The new drug discovery process has been difficult due to very little knowledge about the molecular mechanism involved in SARS-CoV-2 infection (De et al., 2021). There are currently several approved vaccines for COVID-19 and few newly approved therapies, with many potential treatments being evaluated in ongoing clinical trials. These include repurposing the existing drugs previously approved for other conditions, as well as novel biological products (Artese et al., 2020; Drożdżal et al., 2020; Twomey et al., 2020). In this sense, many possible therapies have been pre-clinically and clinically tested against the disease, and many more are in process; however, only a few were found to be effective.

The urgency to make life-saving treatments for COVID-19 available precludes traditional drug discovery paths, given their typically protracted timelines. New drugs to treat SARS-CoV-2 may include either virus or host targets with the potential to block virus infection or viral replication or to modulate the host response to infection (Grobler et al., 2020). Immunotherapies with hyperimmune sera have been applied as a therapeutic approach in the treatment of coronavirus since 2005 (da Costa et al., 2021), and the development of an equine serum with fractions of F(ab')2 for therapeutic use in SARS was already reported in 2005 (Lu et al., 2005). In this study, we systematically evaluated the

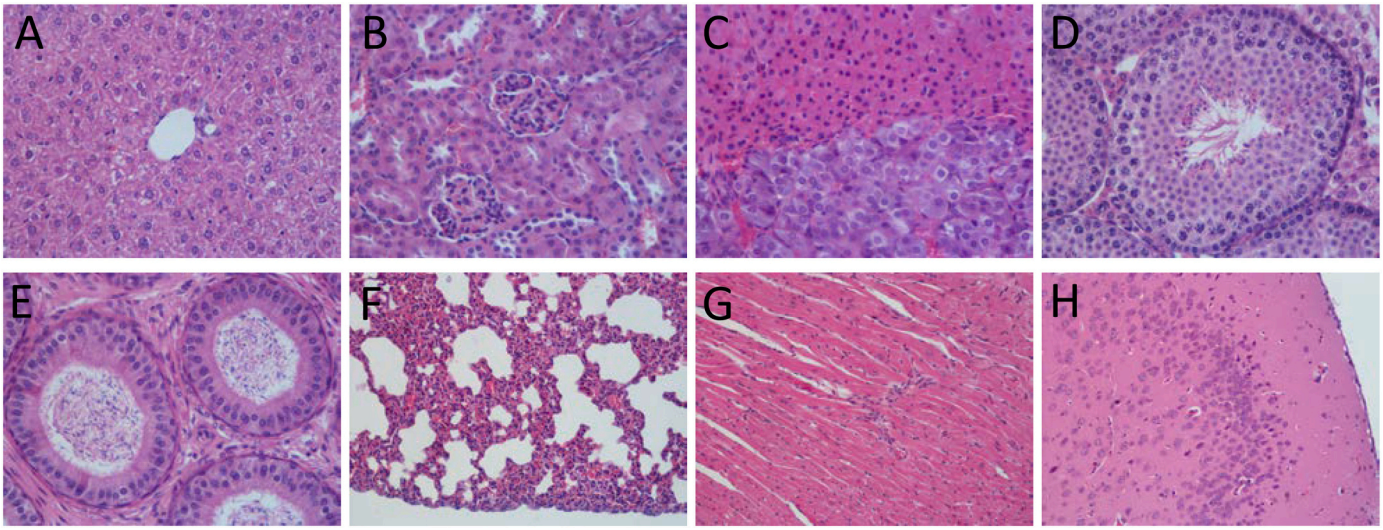


**Fig. 4.** Representative histological images of (A) liver, (B) kidney, (C) adrenal, (D) testis, (E) epididymis, (F) lung, (G) heart and (H) brain from mice treated with of a dose of 4 mg/kg of CoviFab at time 0 and 48 h, and sacrificed at 144 h.

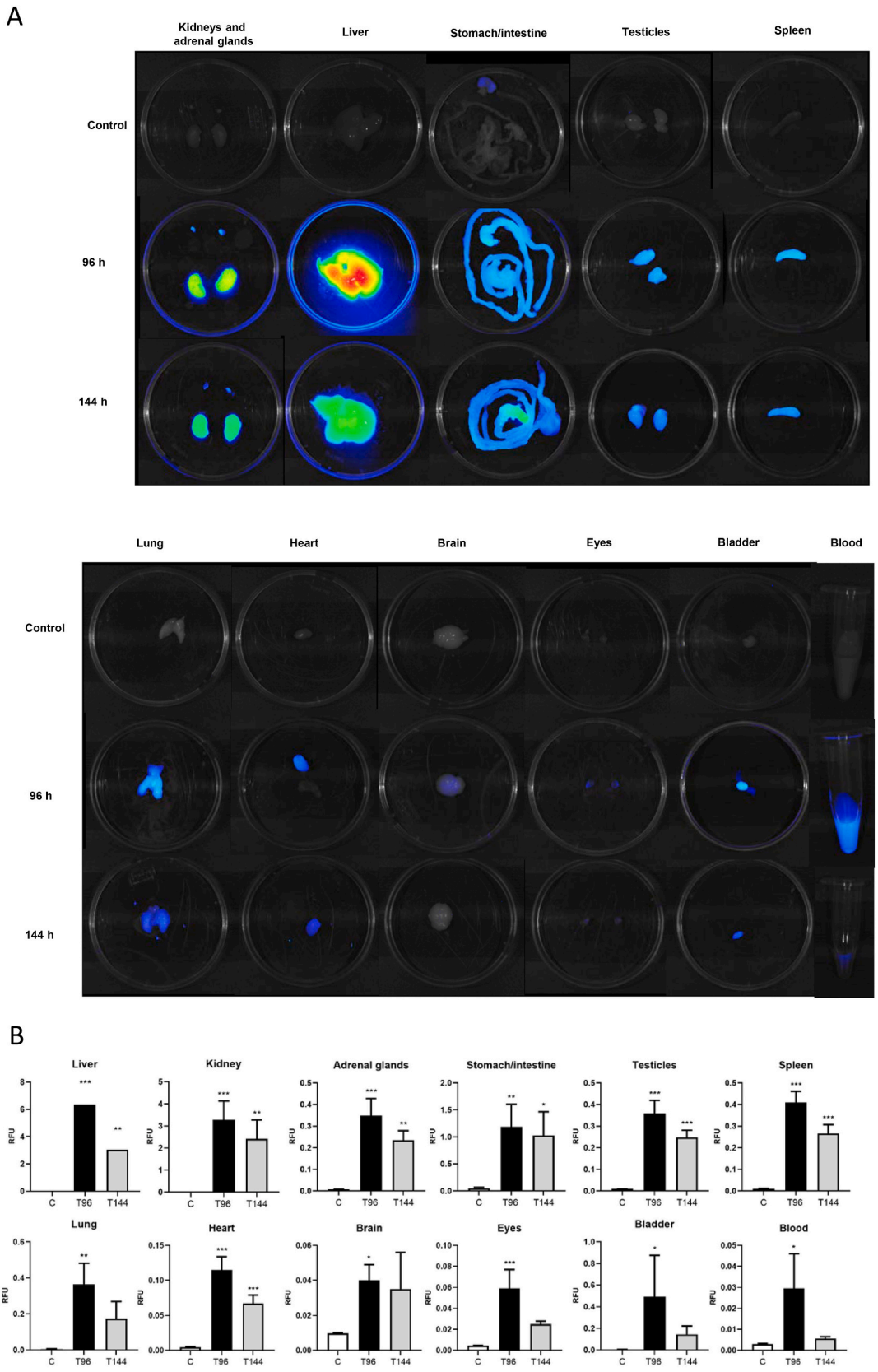


**Fig. 5.** *Ex vivo* fluorescence images in mice treated with CoviFab labelled with IRDye® 800CW, after the administration of intravenous doses of 4 mg/kg at time 0 and at 48 h. A: Representative pseudocolour images of the liver, kidney, adrenal glands, digestive system, testicles, spleen, lung, heart, brain, eyes, bladder, and blood acquired from the control animals (C) and treated animals at 96 h (T96) and 144 h (T144) at necropsies. B: The fluorescence (RFU: relatives fluorescence units) was quantitatively measured in the different organs. Data are presented as mean ± standard deviations. Significant differences with vehicle control group (analysis of variance, Dunnett post hoc test) are indicated (* = $p < 0.05$; ** = $p < 0.01$; *** = $p < 0.001$).

**Table 3**
Haematology parameters of mice treated with CoviFab and controls.

| Parameter | Control animals (n = 5) | Treated animals | |
|---|---|---|---|
| | | 96 h (n = 8) | 144 h (n = 4) |
| RBC ($\times 10^6$/μL) | 9.60 ± 0.57 | 8.98 ± 0.69 | 8.89 ± 0.88 |
| HGB (g/dL) | 12.18 ± 0.79 | 11.61 ± 0.96 | 11.60 ± 0.32 |
| HCT (%) | 51.51 ± 2.28 | 46.26 ± 4.05 | 45.60 ± 5.21 |
| MCV (fL) | 53.66 ± 2.05 | 51.53 ± 1.88 | 51.4 ± 0.9 |
| MCH (pg) | 12.66 ± 0.24 | 12.89 ± 0.35 | 13.12 ± 1.03 |
| MCHC (mg/dL) | 23.65 ± 1.11 | 25.18 ± 1.14 | 25.60 ± 2.30 |
| PLT($\times 10^3$/μL) | 322.37 ± 298.70 | 498.00 ± 312.92 | 598.00 ± 210.62 |
| WBC ($\times 10^3$/μL) | 1.725 ± 0.392 | 2.763 ± 0.920 | 3.180 ± 1.184 |
| GRA ($\times 10^3$/μL) | 0.461 ± 0.169 | 0.695 ± 0.112 | 0.913 ± 0.521 |
| LYM ($\times 10^3$/μL) | 1.218 ± 0.273 | 2.001 ± 0.800 | 2.178 ± 0.548 |
| MNO ($\times 10^3$/μL) | 0.045 ± 0.014 | 0.067 ± 0.024 | 0.088 ± 0.051 |

RBC: red blood cells, HGB: haemoglobin, HCT: haematocrit, MCV: mean cell volume of red blood cells, MCH: mean cell haemoglobin, MCHC: mean corpuscular haemoglobin concentration, PLT: platelet, WBC: white blood cell, GRA: granulocyte, LYM: lymphocyte, MNO: monocyte.
Data are presented as mean ± standard deviations. No statistically significant differences compared with the vehicle control group at $P < 0.05$ were observed (analysis of variance, Dunnett post hoc test).

**Table 4**
Serum chemistry analyses of mice treated with CoviFab and controls and serum concentration of equine F(ab′)2 measured by ELISA.

| Parameter | Control animals (n = 5) | Treated animals | |
|---|---|---|---|
| | | 96 h (n = 4) | 144 h (n = 4) |
| BUN (mg/dl) | 26.45 ± 3.01 | 24.61 ± 2.42 | 26.88 ± 3.54 |
| CRE (mg/dl) | 1.23 ± 0.70 | 0.93 ± 0.33 | 0.97 ± 1.02 |
| ALT (UI/l) | 40.78 ± 9.21 | 40.00 ± 19.05 | 26.25 ± 13.59 |
| AST (UI/l) | 153.03 ± 59.79 | 168 ± 68 | 143 ± 81 |
| TP (g/dl) | 4.68 ± 0.63 | 4.50 ± 0.22 | 4.49 ± 0.21 |
| ALB (g/dl) | 3.11 ± 0.17 | 3.38 ± 0.38 | 3.04 ± 0.33 |
| GLO (g/dl) | 1.56 ± 0.54 | 1.12 ± 0.46 | 1.45 ± 0.38 |
| GLU (g/dl) | 129.94 ± 16.16 | 148.93 ± 30.81 | 145.04 ± 24.74 |
| F(ab′)2 (mg/L) | – | 17.07 ± 3.40 | 6.10 ± 1.25 |

BUN: blood urea nitrogen, CRE: creatinine, ALT: alanine aminotransferase, AST: aspartate aminotransferase, TP: total protein, ALB: albumin, GLO: globulins, GLU: glucose.
Data are presented as mean ± standard deviations. In serum chemistry values, no statistically significant differences compared with the vehicle control group at $P < 0.05$ were observed (analysis of variance, Dunnett post hoc test).

biodistribution and safety of CoviFab using an alternative method based on *in vivo* imaging, a more rapid approach than classical biodistribution used in traditional drug discovery and development, and one better suited for a pandemic response.

An animal model can provide useful data to understand safety, pharmacokinetic, and pharmacodynamic parameters of new biochemically similar molecules. This information may be required to advance to clinic investigation phases. In this sense, *in vivo* optical imaging enables the non-invasive study of molecular targets inside the living animal's body, allowing to analyse the distribution, metabolism, and excretion of labelled molecules.

*In vivo* molecular imaging has become a valuable tool in biomedical research and drug development (Gong et al., 2010; Weissleder and Pittet, 2008; Willmann et al., 2008). In particular, fluorescence optical imaging is becoming a new standard owing to its low cost, ease of use, longer time window for image capture, and ability to simultaneously track multiple probes. Compared with the visible spectrum, the NIR fluorochrome reduces the autofluorescence, maximises tissue penetration, and is ideal for non-invasive animal imaging (Tolmachev et al., 2009; Weissleder, 2001). In this study, CoviFab molecules were labelled with organic IRDye 800CW fluorescent dyes and characterised for *in vivo* and *ex vivo* optical imaging. An advantage of the IRDye 800CW is that both the excitation and emission wavelengths (774 and 805 nm) are centred at a wavelength amenable to intraoperative imaging, which allows deeper tissue penetration of both excitation and emission photons (Huang et al., 2012). Also, the toxicity of IRDye 800CW dye has been tested in a preclinical model, with good results (Marshall et al., 2010). The stable signal of the fluorescent dye also makes it suitable for longitudinal monitoring of probe distribution and clearance over time.

The *in vivo* study showed that CoviFab was rapidly localised in all analysed regions after intravenous injection. In kidney and bladder areas, labelled CoviFab was clearly visualised after 24 h of each injection, with a significantly higher fluorescence in relation to basal. Moreover, in the liver and ears, the fluorescence was major than basal in the complete study period. In all organs, the profile was similar to the highest fluorescence 1 h after each injection, gradually decreasing until the end of the study. The highest relative fluorescence was observed in the kidney and bladder areas, indicating that this could be the main route of excretion, which was later confirmed by the fluorescence values observed in urine, although this fluorescence could be partially due to cleavage of the fluorophore. The *ex vivo* imaging study support the information on the biodistribution determined *in vivo*, allowing to confirm that in most organs, the product remains for more than 144 h after the first administration (96 h after the second administration). This long circulation persistence time is consistent with that described for mono and polyclonal antibodies (Hernot et al., 2019; Joshi and Wang, 2018; Kleinmanns et al., 2020). Our correlation analysis between the *ex vivo* fluorescence of organs, fluorescence analysis of urine and faeces, and serum F(ab′)2 concentration shows that *in vivo* imaging is a strong predictor of biodistribution in pharmacokinetic studies.

In the toxicology study, the intravenous administration of CoviFab at a dose of 4 mg/kg in healthy mice revealed no significant changes in serum biochemical and haematological analyses within 96 and 144 h of observation. Further, there were no changes shown in gross examination of organs during the necropsy and tissue/organ collection process. In addition, the relative organ weights were similar between the treated animals and the respective control animals.

The safety profile was in general similar to NEAST F(ab′)2 fragment antibodies (Hiriart et al., 2019), and these preclinical results are in agreement with the excellent safety profile shown by polyclonal F(ab)2 fragments from equine immunoglobulins currently in medical use. As previously mentioned, a similar strategy was followed during the production of NEAST, which demonstrated to be a safe product. From a regulatory point of view, health authorities might consider that the obtained anti-SARS-CoV-2 F(ab′)2 antisera should be similar to NEAST since both products only differ in their specificities, and the safety of this type of products has been extensively demonstrated (Boyer et al., 2013; Hiriart et al., 2019; Zylberman et al., 2020). Thus, it can be considered that, as both products were manufactured using the same platform and have similar compositions, under the circumstances of a pandemic, the anti-SARS-CoV-2 F(ab′)2 antisera advanced quickly towards its clinical trials and approval by the argentine health authorities, allowing the rapid use of this product during this emergency (Lopardo et al., 2021).

In conclusion, preclinical data of the current study suggest that CoviFab is safe, without observable adverse effects in mice. Moreover, the data obtained by *in vivo* and *ex vivo* NIR imaging indicate their location and permanence in the organs of interest for COVID-19.

## Funding

This study was supported by a grant from the Universidad Nacional del Litoral and from the Agencia Nacional de Promoción de la Investigación, el Desarrollo Tecnológico y la Innovación of the Ministerio de Ciencia, Tecnología e Innovación de Argentina.

## Declaration of Competing Interest

The authors declare that they have no competing financial interests

**Table 5**
Correlation matrix of *ex vivo* fluorescence of organs, fluorescence analysis of urine and faeces, and serum F(ab′)2 at basal, 96 and 144 h. (Pearson correlation coefficients (r) of 12 samples per variable).

| Variables | Ex vivo fluorescence (RFU) | | | | | | | | | | | | Fluorescence analysis (RFU) | | ELISA (mg/L) |
|---|---|---|---|---|---|---|---|---|---|---|---|---|---|---|---|
| | Liver | Kidney | Adrenal glands | Stomach/ intestine | Testicles | Spleen | Lung | Heart | Brain | Eyes | Bladder | Blood | Urine | Faeces | Serum F (ab′)2 |
| Liver | 1.00 | | | | | | | | | | | | | | |
| Kidney | 0.96 | 1.00 | | | | | | | | | | | | | |
| Adrenal glands | 0.98 | 1.00[a] | 1.00 | | | | | | | | | | | | |
| Stomach/ intestine | 0.91 | 0.99[a] | 0.98 | 1.00 | | | | | | | | | | | |
| Testicles | 0.97 | 1.00[a] | 1.00[b] | 0.98 | 1.00 | | | | | | | | | | |
| Spleen | 0.98 | 0.99[a] | 1.00[b] | 0.97 | 1.00[a] | 1.00 | | | | | | | | | |
| Lung | 1.00[b] | 0.96 | 0.97 | 0.91 | 0.97 | 0.98 | 1.00 | | | | | | | | |
| Heart | 1.00[a] | 0.98 | 0.99[a] | 0.95 | 0.99 | 1.00[a] | 0.99[a] | 1.00 | | | | | | | |
| Brain | 0.92 | 0.99[a] | 0.98 | 1.00[b] | 0.99 | 0.98 | 0.92 | 0.95 | 1.00 | | | | | | |
| Eyes | 0.99[a] | 0.92 | 0.95 | 0.86 | 0.94 | 0.96 | 1.00[a] | 0.98 | 0.88 | 1.00 | | | | | |
| Bladder | 0.98 | 0.87 | 0.91 | 0.80 | 0.90 | 0.92 | 0.98 | 0.95 | 0.82 | 0.99[a] | 1.00 | | | | |
| Blood | 0.92 | 0.77 | 0.81 | 0.68 | 0.80 | 0.83 | 0.92 | 0.88 | 0.70 | 0.96 | 0.98 | 1.00 | | | |
| Urine | 0.94 | 0.80 | 0.84 | 0.71 | 0.83 | 0.85 | 0.94 | 0.90 | 0.73 | 0.97 | 0.99[a] | 1.00[a] | 1.00 | | |
| Feaces | 0.94 | 0.79 | 0.84 | 0.71 | 0.83 | 0.85 | 0.94 | 0.90 | 0.73 | 0.97 | 0.99[a] | 1.00[a] | 1.00[b] | 1.00 | |
| Serum F (ab′)2 | 1.00[a] | 0.93 | 0.96 | 0.88 | 0.95 | 0.96 | 1.00[a] | 0.98[a] | 0.92 | 1.00[b] | 0.99 | 0.95[a] | 0.98 | 0.96 | 1.00 |

[a] Correlation is significant at 0.05 level (2-tailed).
[b] Correlation is significant at 0.01 level (2-tailed).

or personal relationships that could have appeared to influence the work reported in this paper. Santiago Sanguineti; Fernando Goldbaum; Luciana Muñoz and Vanesa Zylberman are employees at Inmunova S.A.

## Acknowledgements

We are grateful to the staff members of the Centro de Medicina Comparada (ICiVet-Litoral, UNL-CONICET) for their technical support during the sample processing.

## References

Amanat, F., Stadlbauer, D., Strohmeier, S., Nguyen, T.H.O., Chromikova, V., McMahon, M., Jiang, K., Arunkumar, G.A., Jurczyszak, D., Polanco, J., Bermudez-Gonzalez, M., Kleiner, G., Aydillo, T., Miorin, L., Fierer, D.S., Lugo, L.A., Kojic, E.M., Stoever, J., Liu, S.T.H., Cunningham-Rundles, C., Felgner, P.L., Moran, T., García-Sastre, A., Caplivski, D., Cheng, A.C., Kedzierska, K., Vapalahti, O., Hepojoki, J.M., Simon, V., Krammer, F., 2020. A serological assay to detect SARS-CoV-2 seroconversion in humans. Nat. Med. 26, 1033–1036. https://doi.org/10.1038/s41591-020-0913-5.

Artese, A., Svicher, V., Costa, G., Salpini, R., Di Maio, V.C., Alkhatib, M., Ambrosio, F.A., Santoro, M.M., Assaraf, Y.G., Alcaro, S., Ceccherini-Silberstein, F., 2020. Current status of antivirals and druggable targets of SARS CoV-2 and other human pathogenic coronaviruses. Drug Resist. Updat. 53, 100721. https://doi.org/10.1016/j.drup.2020.100721.

Bal, C., Herbreteau, C.H., Buchy, P., Rith, S., Zaid, M., Kristanto, W., Han, V., Reynaud, C., Granjard, P., Lépine, B., Durand, C., Tambyah, P.A., 2015. Safety, potential efficacy, and pharmacokinetics of specific polyclonal immunoglobulin F (ab′)2 fragments against avian influenza A (H5N1) in healthy volunteers: a single-centre, randomised, double-blind, placebo-controlled, phase 1 study. Lancet Infect. Dis. 15, 285–292. https://doi.org/10.1016/S1473-3099(14)71072-2.

Bayat, M., Asemani, Y., Mohammadi, M.R., Sanaei, M., Namvarpour, M., Eftekhari, R., 2021. An overview of some potential immunotherapeutic options against COVID-19. Int. Immunopharmacol. 95, 107516. https://doi.org/10.1016/j.intimp.2021.107516.

Berry, J.D., Gaudet, R.G., 2011. Antibodies in infectious diseases: polyclonals, monoclonals and niche biotechnology. New Biotechnol. https://doi.org/10.1016/j.nbt.2011.03.018.

Bonam, S.R., Kaveri, S.V., Sakuntabhai, A., Gilardin, L., Bayry, J., 2020. Adjunct immunotherapies for the management of severely Ill COVID-19 Patients. Cell Rep. Med. https://doi.org/10.1016/j.xcrm.2020.100016.

Boyer, L., Degan, J., Ruha, A.-M., Mallie, J., Mangin, E., Alagón, A., 2013. Safety of intravenous equine F(ab′)2: insights following clinical trials involving 1534 recipients of scorpion antivenom. Toxicon 76, 386–393. https://doi.org/10.1016/j.toxicon.2013.07.017.

Chai, K.L., Valk, S.J., Piechotta, V., Kimber, C., Monsef, I., Doree, C., Wood, E.M., Lamikanra, A.A., Roberts, D.J., McQuilten, Z., So-Osman, C., Estcourt, L.J., Skoetz, N., 2020. Convalescent plasma or hyperimmune immunoglobulin for people with COVID-19: a living systematic review. Cochrane Database Syst. Rev. 10, CD013600 https://doi.org/10.1002/14651858.CD013600.pub3.

Choy, K.T., Wong, A.Y.L., Kaewpreedee, P., Sia, S.F., Chen, D., Hui, K.P.Y., Chu, D.K.W., Chan, M.C.W., Cheung, P.P.H., Huang, X., Peiris, M., Yen, H.L., 2020. Remdesivir, lopinavir, emetine, and homoharringtonine inhibit SARS-CoV-2 replication in vitro. Antivir. Res. 178 https://doi.org/10.1016/j.antiviral.2020.104786.

da Costa, C.B.P., Martins, F.J., da Cunha, L.E.R., Ratcliffe, N.A., Cisne de Paula, R., Castro, H.C., 2021. COVID-19 and Hyperimmune sera: a feasible plan B to fight against coronavirus. Int. Immunopharmacol. 90, 107220. https://doi.org/10.1016/j.intimp.2020.107220.

De, P., Chakraborty, I., Karna, B., Mazumder, N., 2021. Brief review on repurposed drugs and vaccines for possible treatment of COVID-19. Eur. J. Pharmacol. 898, 173977. https://doi.org/10.1016/j.ejphar.2021.173977.

Drożdżal, S., Rosik, J., Lechowicz, K., Machaj, F., Kotfis, K., Ghavami, S., Łos, M.J., 2020. FDA approved drugs with pharmacotherapeutic potential for SARS-CoV-2 (COVID-19) therapy. Drug Resist. Updat. 53, 100719. https://doi.org/10.1016/j.drup.2020.100719.

Farrugia, A., MacPherson, J., Busch, M.P., 2020. Convalescent plasma – this is no time for competition. Transfusion. https://doi.org/10.1111/trf.15922.

FDA, 2018. Bioanalytical Method Validation Guidance. Food Drug Adm.

Gasparyan, A.Y., Misra, D.P., Yessirkepov, M., Zimba, O., 2020. Perspectives of immune therapy in coronavirus disease 2019. J. Korean Med. Sci. https://doi.org/10.3346/JKMS.2020.35.E176.

Gong, H., Kovar, J., Little, G., Chen, H., Olive, D.M., 2010. In vivo imaging of xenograft tumors using an epidermal growth factor receptor-specific affibody molecule labeled with a near-infrared fluorophore. Neoplasia 12, 139–IN9. https://doi.org/10.1593/neo.91446.

Grobler, J.A., Anderson, A.S., Fernandes, P., Diamond, M.S., Colvis, C.M., Menetski, J.P., Alvarez, R.M., Young, J.A.T., Carter, K.L., 2020. Accelerated preclinical paths to support rapid development of COVID-19 therapeutics. Cell Host Microbe 28, 638–645. https://doi.org/10.1016/j.chom.2020.09.017.

Gupta, D., Sahoo, A.K., Singh, A., 2020. Ivermectin: potential candidate for the treatment of Covid 19. Brazil. J. Infect. Dis. 24, 369–371. https://doi.org/10.1016/j.bjid.2020.06.002.

Heidary, F., Gharebaghi, R., 2020. Ivermectin: a systematic review from antiviral effects to COVID-19 complementary regimen. J. Antibiot. (Tokyo). https://doi.org/10.1038/s41429-020-0336-z.

Herbreteau, C.H., Jacquot, F., Rith, S., Vacher, L., Nguyen, L., Carbonnelle, C., Lotteau, V., Jolivet, M., Raoul, H., Buchy, P., Saluzzo, J.-F., 2014. Specific polyclonal F(ab′) 2 neutralize a large panel of highly pathogenic avian influenza A viruses (H5N1) and control infection in mice. Immunotherapy 6, 699–708. https://doi.org/10.2217/imt.14.40.

Hernot, S., van Manen, L., Debie, P., Mieog, J.S.D., Vahrmeijer, A.L., 2019. Latest developments in molecular tracers for fluorescence image-guided cancer surgery. Lancet Oncol. 20, e354–e367. https://doi.org/10.1016/S1470-2045(19)30317-1.

Hiriart, Y., Pardo, R., Bukata, L., Lauche, C., Muñoz, L., Berengeno, A., Colonna, M., Ortega, H.H., Goldbaum, F.A., Sanguineti, S., Zylberman, V., 2019. Preclinical studies of NEAST (Neutralizing Equine Anti-Shiga To xin): a potential treatment for prevention of Stec-Hus. Int. J. Drug Dev. Res. 11 https://doi.org/10.36648/0975-9344.11.3.140.

Huang, R., Vider, J., Kovar, J.L., Olive, D.M., Mellinghoff, I.K., Mayer-Kuckuk, P., Kircher, M.F., Blasberg, R.G., 2012. Integrin α v β 3 -targeted IRDye 800CW near-

infrared imaging of glioblastoma. Clin. Cancer Res. 18, 5731–5740. https://doi.org/10.1158/1078-0432.CCR-12-0374.

Jiménez-Alberto, A., Ribas-Aparicio, R.M., Aparicio-Ozores, G., Castelán-Vega, J.A., 2020. Virtual screening of approved drugs as potential SARS-CoV-2 main protease inhibitors. Comput. Biol. Chem. 88 https://doi.org/10.1016/j.compbiolchem.2020.107325.

Joshi, B.P., Wang, T.D., 2018. Targeted optical imaging agents in cancer: focus on clinical applications. Contrast Med. Mol. Imag. 2018, 1–19. https://doi.org/10.1155/2018/2015237.

Khan, S.A., Zia, K., Ashraf, S., Uddin, R., Ul-Haq, Z., 2020. Identification of chymotrypsin-like protease inhibitors of SARS-CoV-2 via integrated computational approach. J. Biomol. Struct. Dyn. https://doi.org/10.1080/07391102.2020.1751298.

Kleinmanns, K., Bischof, K., Anandan, S., Popa, M., Akslen, L.A., Fosse, V., Karlsen, I.T., Gjertsen, B.T., Bjørge, L., McCormack, E., 2020. CD24-targeted fluorescence imaging in patient-derived xenograft models of high-grade serous ovarian carcinoma. EBioMedicine 56, 102782. https://doi.org/10.1016/j.ebiom.2020.102782.

Lang, J., Attanath, P., Quiambao, B., Singhasivanon, V., Chanthavanich, P., Montalban, C., Lutsch, C., Pepin-Covatta, S., Le Mener, V., Miranda, M., Sabchareon, A., 1998. Evaluation of the safety, immunogenicity, and pharmacokinetic profile of a new, highly purified, heat-treated equine rabies immunoglobulin, administered either alone or in association with a purified, Vero-cell rabies vaccine. Acta Trop. 70, 317–333. https://doi.org/10.1016/S0001-706X(98)00038-2.

Lee, W.S., Wheatley, A.K., Kent, S.J., DeKosky, B.J., 2020 Oct. Antibody-dependent enhancement and SARS-CoV-2 vaccines and therapies. Nat Microbiol 5 (10), 1185–1191. https://doi.org/10.1038/s41564-020-00789-5. Epub 2020 Sep 9. PMID: 32908214.

Li, H., Chen, C., Hu, F., Wang, J., Zhao, Q., Gale, R.P., Liang, Y., 2020. Impact of corticosteroid therapy on outcomes of persons with SARS-CoV-2, SARS-CoV, or MERS-CoV infection: a systematic review and meta-analysis. Leukemia 34, 1503–1511. https://doi.org/10.1038/s41375-020-0848-3.

Liu, L., Wei, Q., Lin, Q., Fang, J., Wang, H., Kwok, H., Tang, H., Nishiura, K., Peng, J., Tan, Z., Wu, T., Cheung, K.W., Chan, K.H., Alvarez, X., Qin, C., Lackner, A., Perlman, S., Yuen, K.Y., Chen, Z., 2019 Feb 21. Anti-spike IgG causes severe acute lung injury by skewing macrophage responses during acute SARS-CoV infection. JCI Insight 4 (4), e123158. https://doi.org/10.1172/jci.insight.123158. PMID: 30830861; PMCID: PMC6478436.

Lopardo, G., Belloso, W.H., Nannini, E., Colonna, M., Sanguineti, S., Zylberman, V., Muñoz, L., Dobarro, M., Lebersztein, G., Farina, J., Vidiella, G., Bertetti, A., Crudo, F., Alzogaray, M.F., Barcelona, L., Teijeiro, R., Lambert, S., Scublinsky, D., Iacono, M., Stanek, V., Solari, R., Casas, M.M., Abusamra, L., Luciardi, H.L., Cremona, A., Caruso, D., de Miguel, B., Perez Lloret, S., Millán, S., Kilstein, Y., Pereiro, A., Sued, O., Cahn, P., Spatz, L., Goldbaum, F., 2021. RBD-specific polyclonal F(ab′) $_2$ fragments of equine antibodies in patients with moderate to severe COVID-19 disease: a randomized, double-blind, placebo-controlled, adaptive phase 2/3 clinical trial. SSRN Electron. J. https://doi.org/10.2139/ssrn.3768544.

Lotfi, M., Hamblin, M.R., Rezaei, N., 2020. COVID-19: Transmission, prevention, and potential therapeutic opportunities. Clin. Chim. Acta 508, 254–266. https://doi.org/10.1016/j.cca.2020.05.044.

Lu, J., Guo, Z., Han, W., Wang, G., Zhang, D., Wang, Y., Sun, S., Yang, Q., Zheng, H., Wong, B.L., Zhong, N., 2005. Preparation and development of equine hyperimmune globulin F(ab′)2 against severe acute respiratory syndrome coronavirus1. Acta Pharmacol. Sin. 26, 1479–1484. https://doi.org/10.1111/j.1745-7254.2005.00210.x.

Marshall, M.V., Draney, D., Sevick-Muraca, E.M., Olive, D.M., 2010. Single-dose intravenous toxicity study of IRDye 800CW in Sprague-Dawley rats. Mol. Imaging Biol. 12, 583–594. https://doi.org/10.1007/s11307-010-0317-x.

National Research Council (US), 2011. Committee for the Update of the Guide for the Care and Use of Laboratory Animals. Guide for the Care and Use of Laboratory Animals. 8th ed. Washington (DC): National Academies Press (US). PMID: 21595115.

Pizzorno, A., Padey, B., Dubois, J., Julien, T., Traversier, A., Dulière, V., Brun, P., Lina, B., Rosa-Calatrava, M., Terrier, O., 2020. In vitro evaluation of antiviral activity of single and combined repurposable drugs against SARS-CoV-2. Antiviral Res. 181. https://doi.org/10.1016/j.antiviral.2020.104878.

Quiambao, B.P., DyTioco, H.Z., Dizon, R.M., Crisostomo, M.E., Laot, T.M., Teuwen, D.E., 2008. Rabies post-exposure prophylaxis in the philippines: health status of patients having received purified equine F(ab′)2 fragment rabies immunoglobulin (Favirab). PLoS Negl. Trop. Dis. 2, e243 https://doi.org/10.1371/journal.pntd.0000243.

Sallard, E., Belhadi, D., Lescure, F.X., Yazdanpanah, Y., Peiffer-Smadja, N., 2020a. Clinical trial protocols of repurposed prophylaxis for COVID-19: a review. Med. Mal. Infect. https://doi.org/10.1016/j.medmal.2020.09.013.

Sallard, Erwan, Lescure, F.X., Yazdanpanah, Y., Mentre, F., Peiffer-Smadja, N., 2020b. Type 1 interferons as a potential treatment against COVID-19. Antivir. Res. 178 https://doi.org/10.1016/j.antiviral.2020.104791.

Shannon, A., Le, N.T.-T., Selisko, B., Eydoux, C., Alvarez, K., Guillemot, J.-C., Decroly, E., Peersen, O., Ferron, F., Canard, B., 2020. Remdesivir and SARS-CoV-2: structural requirements at both nsp12 RdRp and nsp14 Exonuclease active-sites. Antivir. Res. 178, 104793. https://doi.org/10.1016/j.antiviral.2020.104793.

Simonovich, V.A., Burgos Pratx, L.D., Scibona, P., Beruto, M.V., Vallone, M.G., Vázquez, C., Savoy, N., Giunta, D.H., Pérez, L.G., Sánchez, M.D.L., Gamarnik, A.V., Ojeda, D.S., Santoro, D.M., Camino, P.J., Antelo, S., Rainero, K., Vidiella, G.P., Miyazaki, E.A., Cornistein, W., Trabadelo, O.A., Ross, F.M., Spotti, M., Funtowicz, G., Scordo, W.E., Losso, M.H., Ferniot, I., Pardo, P.E., Rodriguez, E., Rucci, P., Pasquali, J., Fuentes, N.A., Esperatti, M., Speroni, G.A., Nannini, E.C., Matteaccio, A., Michelangelo, H.G., Follmann, D., Lane, H.C., Belloso, W.H., Group, PlasmAr Study, 2021. A Randomized Trial of Convalescent Plasma in Covid-19 Severe Pneumonia. N Engl J Med. 384 (7), 619–629. https://doi.org/10.1056/NEJMoa2031304. Epub 2020 Nov 24. PMID: 33232588; PMCID: PMC7722692.

Tolmachev, V., Friedman, M., Sandstrom, M., Eriksson, T.L.J., Rosik, D., Hodik, M., Stahl, S., Frejd, F.Y., Orlova, A., 2009. Affibody molecules for epidermal growth factor receptor targeting in vivo: aspects of dimerization and labeling chemistry. J. Nucl. Med. 50, 274–283. https://doi.org/10.2967/jnumed.108.055525.

Twomey, J.D., Luo, S., Dean, A.Q., Bozza, W.P., Nalli, A., Zhang, B., 2020. COVID-19 update: the race to therapeutic development. Drug Resist. Updat. 53, 100733. https://doi.org/10.1016/j.drup.2020.100733.

Weissleder, R., 2001. A clearer vision for in vivo imaging. Nat. Biotechnol. 19, 316–317. https://doi.org/10.1038/86684.

Weissleder, R., Pittet, M.J., 2008. Imaging in the era of molecular oncology. Nature 452, 580–589. https://doi.org/10.1038/nature06917.

Willmann, J.K., van Bruggen, N., Dinkelborg, L.M., Gambhir, S.S., 2008. Molecular imaging in drug development. Nat. Rev. Drug Discov. 7, 591–607. https://doi.org/10.1038/nrd2290.

Wu F, Yan R, Liu M, Liu Z, Wang Y, Luan D, Wu K, Song Z, Sun T, Ma Y, Zhang Y, Wang Q, Li X, Ji P, Li Y, Li C, Wu Y, Ying T, Wen Y, Jiang S, Zhu T, Lu L, Zhang Y, Zhou Q, Huang J. Antibody-dependent enhancement (ADE) of SARS-CoV-2 infection in recovered COVID-19 patients: studies based on cellular and structural biology analysis. medRxiv 2020.10.08.20209114; doi: https://doi.org/10.1101/2020.10.08.20209114.

Zha, L., Li, S., Pan, L., Tefsen, B., Li, Y., French, N., Chen, L., Yang, G., Villanueva, E.V., 2020. Corticosteroid treatment of patients with coronavirus disease 2019 (COVID-19). Med. J. Aust. 212, 416–420. https://doi.org/10.5694/mja2.50577.

Zhang, B., Liu, S., Tan, T., Huang, W., Dong, Y., Chen, L., Chen, Q., Zhang, L., Zhong, Q., Zhang, X., Zou, Y., Zhang, S., 2020. Treatment with convalescent plasma for critically ill patients with severe acute respiratory syndrome coronavirus 2 infection. Chest 158, e9–e13. https://doi.org/10.1016/j.chest.2020.03.039.

Zylberman, V., Sanguineti, S., Pontoriero, A.V., Higa, S.V., Cerutti, M.L., Seijo, S.M.M., Pardo, R., Muñoz, L., Intrieri, M.E.A., Alzogaray, V.A., Avaro, M.M., Benedetti, E., Berguer, P.M., Bocanera, L., Bukata, L., Bustelo, M.S., Campos, A.M., Colonna, M., Correa, E., Cragnaz, L., Dattero, M.E., Dellafiore, M., Foscaldi, S., González, J.V., Guerra, L.L., Klinke, S., Labanda, M.S., Lauché, C., López, J.C., Martínez, A.M., Otero, L.H., Peyric, E.H., Ponziani, P.F., Ramondino, R., Rinaldi, J., Rodríguez, S., Russo, J.E., Russo, M.L., Saavedra, S.L., Seigelchifer, M., Sosa, S., Vilariño, C., Biscayart, P.L., Corley, E., Spatz, L., Baumeister, E.G., Goldbaum, F.A., 2020. Development of a hyperimmune equine serum therapy for covid-19 in Argentina. Medicina (B. Aires) 80, 1–6.